Double negatively charged carbon vacancy at the h- and k- sites in 4H-SiC: Combined Laplace-DLTS and DFT study

Ivana Capan, Tomislav Brodar
Division of Materials Physics, Rudjer Boskovic Institute, Bijenicka 54, 10 000 Zagreb, Croatia

Željko Pastuović, Rainer Siegele
Centre for Accelerator Science, Australian Nuclear Science and Technology Organisation, 1New Illawarra Rd, Lucas Heights NSW 2234, Australia

Takeshi Ohshima, Shin-ichiro Sato, Takahiro Makino
Takasaki Advanced Radiation Research Institute, National Institutes for Quantum and Radiological Science and Technology, 1233 Watanuki, Takasaki, Gunma 370-1292, Japan

Luka Snoj, Vladimir Radulović
Jožef Stefan Institute, Jamova 39, 1000 Ljubljana, Slovenia

José Coutinho, Vitor J. B. Torres
Department of Physics and I3N, University of Aveiro, Campus Santiago, 3810-193 Aveiro, Portugal

Kamel Demmouche
Institut des Sciences, Centre Universitaire -Belhadj Bouchaib- Ain Temouchent, B.P. 284 46000 Ain Temouchent, Algeria

We present results from combined Laplace-Deep Level Transient Spectroscopy (Laplace-DLTS) and density functional theory (DFT) studies of the carbon vacancy (V_C) in n-type 4*H*-SiC. Using Laplace-DLTS we were able to distinguish two previously unresolved sub-lattice-inequivalent emissions, causing the broad $Z_{1/2}$ peak at 290 K that is commonly observed by conventional DLTS in n-type 4*H*-SiC. This peak has two components with activation energies for electron emission of 0.58 eV and 0.65 eV. We compared these results with the acceptor levels of V_C obtained by means of hybrid density functional supercell calculations. The calculations support the assignment of the $Z_{1/2}$ signal to a superposition of emission peaks from double negatively charged V_C defects. Taking into account the measured and calculated energy levels, the calculated relative stability of V_C in hexagonal (*h*) and cubic (*k*) lattice sites, as well as the observed relative amplitude of the Laplace-DLTS peaks, we assign Z_1 and Z_2 to $V_C(h)$ and $V_C(k)$, respectively. We also present preliminary results of DLTS and Laplace-DLTS measurements on deep level defects (ET1 and ET2) introduced by fast neutron irradiation and He ion implantation in 4*H*-SiC. The origin of ET1 and ET2 is still unclear.

I. INTRODUCTION

Deep level defects that act as charge carrier traps have high importance in semiconductor industry and applications of semiconductor devices. These defects are mainly created during i) semiconductor material growth, ii) processing by ion implantation or iii) operation in a harsh ionizing radiation environment. In this work, we investigate electron emissions from double negatively charged vacancies in 4*H*-SiC, which are important electron traps already present in as-grown material. We also report on defects created in N-doped epitaxial 4*H*-SiC thin layers irradiated with fast neutrons and implanted with accelerated He^{2+} ions using a fast-scanning reduced-rate ion microbeam. Silicon carbide has attracted a lot of attention as a material for power electronics with extremely low loss [1-3]. Besides, silicon carbide is expected to be used in the fabrication of electronic devices with high radiation resistance, capable to be used in accelerators and nuclear facilities, as well as in space applications [4-7].

For the development of SiC-based devices used in radiation environments, it is very important to understand the effects of accumulated radiation damage on the electronic properties of these devices. Therefore, radiation induced defects, especially those limiting the carrier lifetime, and by that way degrading the performance in terms of charge collection efficiency, need to be fully understood. Deep level defects known as $Z_{1/2}$, are known as one of the most stable defects in 4*H*-SiC acting as strong minority carrier recombination centers in n-type material [8-11]. $EH_{6/7}$ carrier traps are also known as stable defects and are observed together with $Z_{1/2}$ in 4*H*-SiC [8-11]. Son *et al.* ascribed both $Z_{1/2}$ and $EH_{6/7}$ to (=/0) and (0/++) transitions from the single carbon vacancy (V_C) in 4*H*-SiC [12]. Despite being able to distinguish V_C defects at *k*- and *h*-sites in the electron paramagnetic resonance (EPR) spectra, i.e. $V_C(k)$ and $V_C(h)$ respectively, conventional deep level transient spectroscopy (DLTS) was not able to resolve the two corresponding defects from the main $Z_{1/2}$ band. Hemmingsson and co-workers [13] had previously connected $Z_{1/2}$ to a pair of metastable acceptor levels, labeled $Z_1(-/0)$ and $Z_2(-/0)$, but despite the efforts there is no hard evidence that the stable $Z_{1/2}$ peak is made of more than one defect configuration. This has limited a direct link between the EPR and DLTS data.

In this paper we report the results of DLTS and Laplace-DLTS studies of deep levels attributed to the carbon vacancy in N-doped 4*H*-SiC. We also report the acceptor levels of V_C by means of hybrid density functional supercell calculations. We show that the negative-*U* ordering of V_C acceptors results from strong atomic relaxations that take place after carrier emissions. The calculations support the assignment of the $Z_{1/2}$ signal to a superposition of emission peaks from double negatively charged V_C defects. Comparison of the calculations with the Laplace-DLTS data allows us to assign inequivalent sub-lattice sites to Z_1 and Z_2.

II. EXPERIMENTAL AND THEORETICAL DETAILS

n-type silicon carbide Schottky barrier diodes (SBDs) were fabricated on nitrogen-doped epitaxial grown 4*H*-SiC single crystal layers approximately 25 μm thick [14]. The Schottky barrier was formed by evaporation of nickel through a metal mask with patterned square apertures of 1 mm × 1 mm, while Ohmic contacts were formed by nickel sintering at 950 °C in Ar atmosphere on the back side of the silicon carbide substrate. A reverse negative bias was connected to the front Schottky contact, while the back Ohmic contact of the 4*H*-SiC SBDs was grounded. The calculated free carrier concentration in pristine samples was ~5×10^{14} cm^{-3} across the thickness of the epitaxial layer, where a −10 V reverse voltage applied for DLTS measurements corresponded to a depletion depth of 4.9 μm.

Samples were irradiated inside Cd thermal neutron filters with a wall thickness of 1 mm in the Pneumatic Tube (F2a4) irradiation location in the 250 kW JSI TRIGA reactor in Ljubljana. The neutron spectrum in the irradiation location was characterized previously on the basis of Monte Carlo calculations with the MCNP code and activation measurements [15,16]. Three power levels (2.5 W, 25 W and 250 kW) were used for neutron irradiations in the 10^8 to 10^{15} cm^{-2} nominal fluence range.

Activation measurements for the $^{197}Au(n,\gamma)$ reaction were performed for each power level activation in order to deduce the total neutron flux. The sub-cadmium flux was obtained from the characterized neutron spectrum and the Cd cut-off energy for the thickness of 1 mm, i.e. 0.55 eV. Table I reports details of the neutron irradiation conditions for the selected samples. The calculated uncertainties in the neutron fluences were obtained from uncertainties in the neutron flux and the irradiation time.

Selected pristine as-prepared samples were pattern implanted with 2 MeV He^{2+} ions using a fast-scanning microbeam at the ANSTO nuclear microprobe facility [17] in order to generate isolated ion collision cascades in the 4*H*-SiC layers. According to SRIM [18] simulations, the stopping range of the He^{2+} implants was approximately 4.7±0.1 μm. This was chosen to obtain an atomic displacement density distribution within the depletion region of the reversely biased SBDs examined using deep-level transient spectroscopy (DLTS).

DLTS measurements were carried out on a Sula Technologies Deep Level Spectrometer in the temperature range up to 380 K, in vacuum and in the absence of light. All DLTS and Laplace-DLTS measurements were done using a reverse bias voltage of −10 V, with a 9.9 V pulse lasting 10 ms. Laplace-DLTS has higher energy resolution (usually a few meV) than conventional DLTS, and has been successful in revealing information on the local environment of defects and impurities, such as strain fields or atomic siting. The Laplace-DLTS spectra were obtained from capacitance transients by the Flog numerical routine. Each calculated spectrum contains 200 points. Capacitance transients were recorded using a Boonton 7000 capacitance meter in temperature range 282-300 K with a 2 K step. At each temperature, capacitance transient measurements took few minutes; sampling rates were in range 8-60 kHz with a total number of samples around 3×10^4.

Density functional calculations were carried out using the VASP code package [19]. We employed the projector-augment wave method to describe the core electrons [20], while a plane-wave basis with kinetic energy up to 400 eV was used to describe the Kohn-Sham electronic states. The exchange-correlation potential was evaluated using the hybrid density functional of Heyd-Scuseria-Ernzerhof (HSE06) [21], which mixes semi-local and exact exchange interactions at short ranges, treating the long-range interactions within the simpler generalized gradient approximation (GGA) [22]. HSE06-level energies were obtained from pre-relaxed defect structures using the GGA for the exchange-correlation energy.

Vacancy defects were inserted in 576-atom supercells, corresponding to 6×6×2 unit cells of 4*H*-SiC with lattice parameters a=3.071 Å and c=10.052 Å, and the Brillouin zone was sampled at **k** = (0 0 1/2). We found this particular sampling scheme to provide energy differences with an error bar of about 5 meV (when compared to results obtained using a 2×2×2 sampling grid). Further, in GGA calculations that used the **k** = (0 0 1/2) point, we did not find artificial hybridizations between defect levels lying high in the gap and the conduction band states. This effect takes place at **k**=Γ due to the underestimation of the band gap width.

Energy levels were obtained by comparing the electron affinity of defective supercells with the same quantity for a bulk supercell. The latter quantity is representative of the conduction band minimum energy. Total energies of charged supercells were adjusted by a periodic charge correction [23].

III. RESULTS AND DISCUSSION

The ground state structures of carbon vacancy (V_C) defects obtained from hybrid density functional calculations are summarized in Figure 1(a). The structure of the vacancy is sensitive to a pseudo-Jahn-Teller effect, which depends on the charge state [24-26]. The Si atoms bordering the vacancy in structures B, C and D, define tetrahedra possessing respectively 2, 1 and 3 Si-Si edges distinctively shorter among a total of 6 [26]. These are represented as thick segments in Fig. 1(a).

For V_C at the k-site we found that irrespectively of the Fermi level location, only $V_C^0(k)$ and $V_C^=(k)$ states are stable (the negative charge state has always higher formation energy than neutral and double minus charge states), and the (=/0) transition takes place at about E_c−0.63 eV. This means that the acceptor levels of $V_C(k)$ show an inverted order (commonly referred to as negative-U ordering).

Metastable transitions involving the V_C^- state, namely E(−/0) and E(=/−) are calculated at E_c−0.61 eV and E_c−0.64 eV, respectively, and can be visualized in the configuration coordinate diagram of Figure 1(b), where it becomes clear that the $V_C^- \rightarrow V_C^0 + e^-$ electronic emission, involves a change from structure D to structure B.

The vacancy at the *h*-site has electronic transitions very close to those of $V_C(k)$. *E*(−/0) and *E*(=/−) levels are calculated at E_c−0.67 eV and E_c−0.64 eV, respectively. We note however, that although in this case the calculated *U*-value is positive, it is nearly zero. Considering a typical error bar of 0.1 eV in the calculation of levels, our results are also consistent with the observation suggesting $V_C(h)$ being a negative-*U* defect like $V_C(k)$ [26]. An important difference between $V_C(k)$ and $V_C(h)$ is the fact that the ground state of $V_C^-(h)$ adopts structure C (while D is now metastable by 0.14 eV). We note that the barriers for C↔D conversion were calculated to be 0.06 eV and 0.17 eV for $V_C^-(k)$ and $V_C^-(h)$, respectively (see Figure 1(b)). This implies that both C and D structures could be involved in the emission process at the temperatures of DLTS measurements (close to 300 K). If that is the case, and structure D of $V_C^-(h)$ is accessible during DLTS measurements, electron emissions from $V_C^=$ and V_C^- are anticipated to have energies of 0.64 eV and 0.53 eV, respectively, and therefore showing a negative-*U* (=/0) level at E_c − 0.59 eV.

We found that the carbon vacancy in 4*H*-SiC is invariably more stable at the *k*-site than at the *h*-site, irrespectively of its charge state. Accordingly, the energies of V_C^0, V_C^-, and $V_C^=$ were found to be 0.13 eV, 0.06 eV, and 0.06 eV lower for site-*k* than for site-*h*. This suggests that in as-grown material, the population of $V_C(k)$ defects should be larger than that of $V_C(h)$.

Figure 2 shows DLTS spectra of as-grown, neutron irradiated and He^{2+} implanted samples. In the as-grown sample, only one peak is observed. The estimated activation energy for electron emission was 0.64 eV. This defect, known as $Z_{1/2}$, has been reported for numerous times as the most dominant defect in as-grown 4*H*-SiC, and was ascribed to the carbon vacancy [12].

The $Z_{1/2}$ DLTS peak has been claimed to result from a superposition of two overlapping peaks associated with Z_1 and Z_2 defects, ascribed to V_C defects on both sub-lattice sites of 4*H*-SiC. It is generally accepted that they are both negative-*U* double acceptors. Indeed, this assignment is strongly supported by our calculated (=/0) levels at E_c−0.63 eV and E_c−0.59 eV for $V_C(k)$ and $V_C(h)$, respectively. However, due to the inherent limitations in the resolution of conventional DLTS, Z_1(=/0) and Z_2(=/0) double-emissions could not be resolved.

The above view means that under equilibrium conditions, V_C defects can trap two electrons but not one. Hence, electron emission proceeds as a two-stage mechanism ($V_C^= \rightarrow V_C^- + e^- \rightarrow V_C^0 + 2e^-$), which cannot be resolved by single-pulse DLTS measurements. Only the emission of the deeper level is detected as the rate-limiting step [27]. The emission of the second and more weakly bound electron could be resolved by applying a double pulse sequence of a short voltage pulse followed by pumping the sample with an optical pulse [13, 28].

We applied the Laplace-DLTS technique in order to resolve Z_1(=/0) and Z_2(=/0) in 4*H*-SiC. In a previous work, Koizumi *et al.* were able to resolve electron emissions from the carbon vacancy at three sites, namely k_1, k_2 and *h*, in the 6*H* polytype of SiC [29]. Here we look at the analogous problem for the unchartered case of $Z_{1/2}$ in 4*H*-SiC.

Figure 3 shows the Laplace-DLTS spectra for the as-grown sample. Two peaks could be clearly separated, and their activation energies for electron emission were determined as E_c − 0.58 eV and E_c − 0.65 eV from the Arrhenius plot shown in Figure 4 of T^2-corrected electron emission rates. These energies are in a good agreement with those reported by Hemmingson *et al* [13], and for the sake of labelling consistency, and based on their relative position in the gap, we respectively refer to them as Z_1 and Z_2. Other physical parameters such as the capture cross section and concentration of both Z_1 and Z_2 have also been calculated from Laplace-DLTS measurements, and are given in the Table II.

Interestingly, we found the $[Z_1]$:$[Z_2]$ intensity ratio to be 1:5, in contrast to 1:1 or 1:2 as previously reported for as-grown 4*H*-SiC samples [13, 28]. Our result suggests that the ratio is likely to depend on growth conditions, thermal history and/or doping of the sample. This is supported by the strong charge-state dependence of the relative stability of $V_C(k)$ and $V_C(h)$ obtained from the DFT calculations.

Ion implantations and fast neutron irradiations have introduced new deep levels which are evidenced by changes in the DLTS spectra as shown in Fig. 2. They could be summarized as follows:

(i) He-ion implantations lead to an increase of the $Z_{1/2}$ peak and to the introduction of an additional peak (labelled as ET1). As the intensity of $Z_{1/2}$ increased with ion fluencies, its peak maximum shifted to higher temperatures (not shown in Fig. 2). A similar shift was already observed in 4*H*-SiC epi-layers irradiated with protons, alpha particles and electrons, and it was interpreted as the release of stress produced by defect clusters [30,31];

(ii) For the neutron fluencies lower than 10^{13} cm^{-2}, no changes were observed (not shown in Fig. 2). For higher fluencies, the intensity of $Z_{1/2}$ slightly increased, and another peak was introduced (labelled as ET2).

ET1 and ET2 traps were previously reported in the literature and were assigned to several defects [13,32]. Their low thermal stability is the only consensual property among the earlier studies. ET1 and ET2 traps might be simple defects with low thermal stability such as carbon interstitials or Frenkel pairs, since they are introduced by different radiation sources and disappear after DLTS measurements up to 700 K [32]. At this point we could not determine the concentration of ET1 and ET2 in a reliable manner. This follows from the fact that ion-implants and fast-neutrons produce highly inhomogeneous damage, which was clearly seen by CV profiling measurements [32].

Additionally, we performed a low-temperature annealing that did not yield any clarification regarding the origin of ET1 and ET2 peaks, but only indicated a rather complex nature of the defects introduced. In a previous study [32], we had shown that annealing treatments at temperature as low as 700 K introduce significant changes in implanted (H and He ions) 4*H*-SiC material, although the calculated activation energies for migration and transformation of intrinsic defects in 4*H*-SiC are considerably high [33]. We also reported that the changes observed in the material during such low temperature annealing treatments, affect the free carrier concentration [32]. The observed recovery of the free carrier concentration has been connected with the transformation of as-implanted induced defects possessing a low thermal stability.

While EPR experiments were successful in distinguishing V_C defects located at *k*- and *h*-sites, that has not been the case with conventional DLTS regarding $Z_{1/2}$. In this respect, the high-resolution provided by Laplace DLTS provides an opportunity to directly compare the calculated levels with the experiments. As reported above, while we calculate a $E(=/0)$ level for $V_C(k)$ at $E_c-0.63$ eV, for $V_C(h)$ we obtain $E(-/0)$ and $E(=/-)$ *ground state* transitions at $E_c-0.67$ eV and $E_c-0.64$ eV (calculated positive-*U* value is close to zero). However, if we consider that after the 0.64 eV emission from $V_C^{=}(h)$, a second emission can immediately follow from structure D to B with an activation energy of 0.53 eV (see Fig. 1(b)), this would result in a negative-*U* peak with energy $E(=/0)$ at $E_c - 0.59$ eV. Hence, our results support the connection of $V_C(k)$ to the 0.65 eV Laplace-DLTS emission (Z_2), while $V_C(h)$ should be assigned to the 0.58 eV peak (see Figs. 3 and 4).

Further, considering that irrespectively of the charge state, $V_C(k)$ is always more stable than $V_C(h)$, and inferring that in the as-grown SiC samples the vacancy concentration is close to equilibrium, the Laplace-DLTS peak related to $V_C(k)$ should have greater amplitude than the analogous peak related to $V_C(h)$. From a direct comparison of the calculated relative energies with the Laplace-DLTS peak amplitudes, we confirm the assignment of Z_1 and Z_2 to electron emissions from $V_C^{=}(h)$ and $V_C^{=}(k)$, respectively. This assignment is also consistent with the EPR measurements from Ref. 12. Here, the $V_C^{-}(h)$ EPR signal was detected in darkness upon heating the sample above 100 K, whereas observation of $V_C^{-}(k)$ always required external illumination. This indicates that when the Fermi level is close to the (=/0) transition, $V_C^{-}(h)$ is almost as stable as other competing charge states, unlike $V_C^{-}(k)$ which must be metastable.

IV. CONCLUSIONS

We report on Laplace-DLTS measurements combined with hybrid density functional calculations of the electronic properties of the carbon vacancy in 4*H*-SiC. Our results demonstrate that at the origin of the $Z_{1/2}$ DLTS band are two defects with close emission rates. These are assigned to Z_1(=/0) and Z_2(=/0) transitions, and they are related to previous optically-pumped dual-pulse DLTS experiments [13,28], which found metastable Z_1(−/0) and Z_2(−/0) peaks. Our work provides hard evidence for the assignment of $Z_{1/2}$ to superimposed (=/0) transitions of V_C located at *k*- and *h*-sites. Combining the calculations with high-resolution Laplace-DLTS data, we finally ascribe a sub-lattice site to each component of $Z_{1/2}$. Accordingly, by correlating measured and calculated energy levels, as well as the calculated relative stability of V_C in both sites with the relative amplitude of the Laplace-DLTS peaks, we assign Z_1 and Z_2 to consecutive two-electron emissions from $V_C^{=}$(*h*) and $V_C^{=}$(*k*), respectively.

The origin of the additional ET1 and ET2 deep level defects introduced by fast neutron irradiation and He-ion implantation remains unclear and will be the subject of following studies.

ACKNOWLEDGMENTS

This work is supported by the NATO SPS programme, project number 985215. The authors wish to acknowledge the National Collaborative Research Infrastructure Strategy (NCRIS) funding provided by the Australian Government for this research. JC would like to thank the support by the Fundação para a Ciência e a Tecnologia (FCT) through project UID/CTM/50025/2013. The epitaxial films used in this study were grown by Central Research Institute of Electric Power Industry (CRIEPI). Authors would like to thank Dr. N. Hoshino and Dr. H. Tsuchida of CRIEPI.

REFERENCES

1. T. Nakamura, M. Miura, N. Kawamoto, Y. Nakano, T. Otsuka, K. Oku-mura, and A. Kamisawa, phys. status solidi (a) **206**, 2403 (2009).
2. P. Friedrichs, T. Kimoto, L. Ley, and G. Pensl, Silicon Carbide Vol. 2: Power Devices and Sensors (Wiley-VCH Verlag GmbH, Weinheim, 2010).
3. T. Kimoto, and J. A. Cooper, Fundamentals of Silicon Carbide Technology: Growth, Characterization, Devices and Applications (IEEE press, John Wiley and Sons, Singapore, 2014).
4. S. Onoda, N. Iwamoto, S. Ono, S. Katakami, M. Arai, K. Kawano, and T. Ohshima, IEEE Trans Nucl. Sci. **56**, 3218 (2009).
5. C. Zhang, E. Zhang, D. M. Fleetwood, R. D. Schrimpf, S. Dhar, S. Ryu, X. Shen, and S. T. Pantelides, IEEE Trans Nucl. Sci. **58**, 2925 (2011).
6. A. Akturk, J. M. McGarrity, S. Potbhare, and N. Goldsman, IEEE Trans Nucl. Sci. **59**, 3258 (2012).
7. T. Ohshima, S. Onoda, N. Iwamoto, T. Makino, M. Arai, and Y. Tanaka, Radiation Response of Silicon Carbide Diodes and Transistors, Chapter 16 of Physics and Technology of Silicon Carbide Devices, Ed. Y. Hijikata (InTech, Rijeka, 2013), p.379.
8. L. Storasta, J. P. Bergman, E. Janzén, A. Henry, J. Lu, J. Appl. Phys. **96**, 4909-4915 (2004).
9. G. Alfieri, E. V. Monakhov, B. G. Svensson, M. K. Linnarsson, J. Appl. Phys. **98**, 043518 (2005).
10. S. Sasaki, K. Kawahara, G. Feng, G. Alfieri, T. Kimoto, J. Appl. Phys. **109**, 013705 (2011).
11. B. Zippelius, J. Suda, T. Kimoto, J. Appl. Phys. **111**, 033515 (2012).
12. 12. N. T. Son, X. T. Trinh, L. S. Lřvlie, B. G. Svensson, K. Kawahara, J. Suda, T. Kimoto, T. Umeda, J. Isoya, T. Makino, T. Ohshima, and E. Janzén, Phys. Rev. Lett. **109**, 187603 (2012).
13. C. G. Hemmingsson, N. T. Son, A. Ellison, J. Zhang, and E. Janzén, Phys. Rev. B **58**(16), R10119 (1998).
14. M. Ito, L. Storasta, and H. Tsuchida, Appl. Phys. Express. **1**, 015001 (2008).
15. L. Snoj *et al.*, Computational analysis of irradiation facilities at the JSI TRIGA reactor, Applied Radiation and Isotopes, Vol. 70, Issue 3, pp. 483-488 (2012).
16. A. Trkov *et al.*, The GRUPINT neutron spectrum adjustment code – general features and characterization of the spectra in three irradiation channels of the JSI TRIGA reactor, International Symposium on Reactor Dosimetry (ISRD-16), 2017, May 7-12, Santa Fe (NM), USA.
17. Z. Pastuovic, R. Siegele, D. D. Cohen, M. Mann, M. Ionescu, D. Button, S. Long, Nucl. Instr. Meth. Phys. Res. B **404**, 1 (2017).
18. SRIM, www.srim.org.
19. G. Kresse and J. Furthmüller, Phys. Rev. B **54**, 11169 (1996).
20. P. E. Blöchl, Phys. Rev. B **50**, 17953 (1994).
21. A. V. Krukau, O. A. Vydrov, A. F. Izmaylov, and G. E. Scuseria, J. Chem. Phys. **125**, 224106 (2006).
22. J. P. Perdew, K. Burke, and M. Ernzerhof, Phys. Rev. Lett. **77**, 3865 (1996).
23. C. Freysoldt, J. Neugebauer, and C. G. Van de Walle, Phys. Rev. Lett. **102**, 016402 (2009).
24. M. Bockstedte, M. Heid, and O. Pankratov, Phys. Rev. B **67**, 193102 (2003).

25. X. T. Trinh, K. Szász, T. Hornos, K. Kawahara, J. Suda, T. Kimoto, Gali, E. Janzén, and N. T. Son, Phys. Rev. B **88**, 235209 (2013).
26. J. Coutinho, V. J. B. Torres, K. Demmouche and S. Öberg, Phys. Rev. B **96**, 174105 (2017).
27. G. D. Watkins, Negative-*U* properties for defects in solids, in Advances in Solid State Physics, edited by P. Grosse (Springer Berlin Heidelberg, Berlin, Heidelberg, 1984) pp. 163-189.
28. I. Pintilie, L. Pintilie, K. Irmscher, and B. Thomas, J. Appl. Phys. **81**, 4841 (2002).
29. A. Koizumi, V. P. Markevich, N. Iwamoto, S. Sasaki, T. Ohshima, K. Kojima, T. Kimoto, K. Uchida, S. Nozaki, B. Hamilton, and A. R. Peaker, Applied Physics Letters **102**, 032104 (2013).
30. Z.Pastuovic, I.Capan, D. D.Cohen, J. Forneris, N. Iwamoto, T. Ohshima, R. Siegele, N. Hoshino, and H. Tsuchida, Nucl. Inst. Meth. Phys. Res. B **348**, 233 (2015).
31. A. Castaldini, A. Cavallini, L. Rigutti, F. Nava, S. Ferrero and F. Giorgis, J. Appl. Phys. **98**, 053706 (2005).
32. Z. Pastuovic, I. Capan, S. Sato, T. Ohshima, T. Brodar and R. Siegele, J. Phys.: Condens. Matter **29**, 475701 (2017).
33. U. Gerstmann, E. Rauls, Th. Frauenheim, and H. Overhof, Phys. Rev. **67**, 205202 (2003).

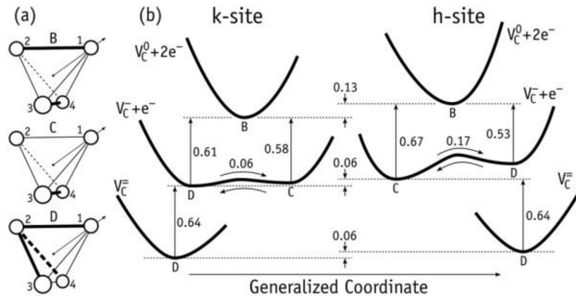

FIG. 1. (a) Diagrams of vacancy structures B, C and D. Shorter Si_i-Si_j distances are shown as thick lines. The arrow passing through Si_1 is parallel to the *c*-axis. (b) Configuration coordinate diagram of V_C in n-type 4*H*-SiC (energies are in eV).

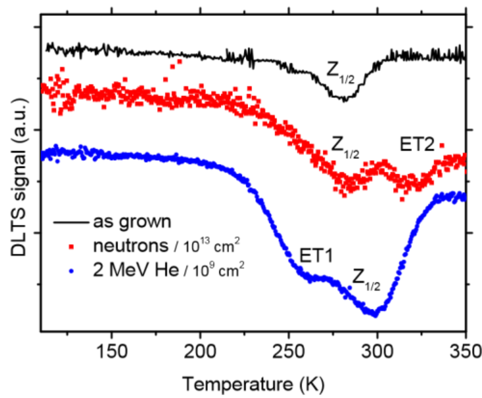

FIG. 2. DLTS spectra of as-grown, as well as selected neutron irradiated and He-ion implanted samples. Measurement settings are reverse bias voltage −10 V, pulse height 9.9 V, pulse width 10 ms and time window 100 ms.

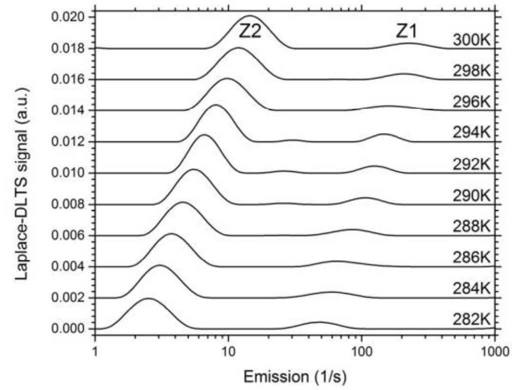

FIG. 3. Laplace-DLTS spectra for an as grown sample measured at temperatures in the range 282-300 K. Measurement settings are reverse bias voltage −10 V, pulse height 9.9 V and pulse width 10 ms.

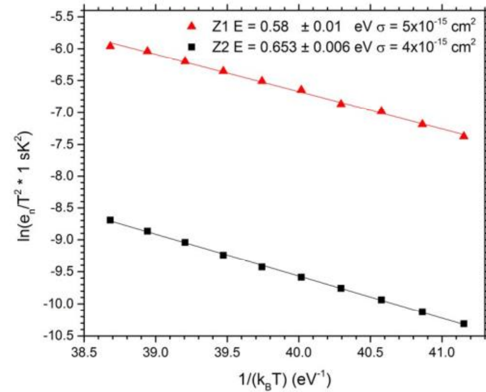

FIG. 4. Arrhenius plots of T^2-corrected electron emission rates for the Z_1 and Z_2 defects observed in the Laplace-DLTS spectrum of the as-grown sample.

Table I. Samples used for this study, neutron irradiation and ion implantation conditions. **Top**: neutron irradiation details (sample ID, irradiation time, reactor power, sub-cadmium neutron flux and uncertainty, sample neutron fluence). **Bottom**: ion implantation details (sample ID, ion type, rate / pixel dwell time, ion energy, fluence).

Sample ID	Irr. Time (s)	Power (W)	Sub-Cd flux (n cm^{-2} s^{-1}), Unc. (%)	Fluence (n cm^{-2}), Unc. (%)
R6	3.0	2.5	3.66×10^{7} (2.7 %)	1.10×10^{8} (9.8 %)
R10	30	2.5	3.66×10^{7} (2.7 %)	1.10×10^{9} (2.9 %)
R11	300	2.5	3.66×10^{7} (2.7 %)	1.10×10^{10} (2.7 %)
R9	273	25	3.44×10^{8} (2.9 %)	9.39×10^{10} (2.9 %)
R12	2730	25	3.44×10^{8} (2.9 %)	9.39×10^{11} (2.9 %)
1E13	2.73	250000	3.66×10^{12} (2.7 %)	1.00×10^{13} (10.7 %)
1E14	27.3	250000	3.66×10^{12} (2.7 %)	1.00×10^{14} (2.9 %)
1E15	273	250000	3.66×10^{12} (2.7 %)	1.00×10^{15} (2.7 %)
Sample ID	Ion	Rate (kHz) / Pixel dwell time (ms)	Ion En. (MeV)	Fluence (cm^{-2})
R1		Pristine		
R13	He^{2+}	5 / 0.1	2.0	5×10^{8}
R14	He^{2+}	5 / 0.1	2.0	1×10^{9}
R15	He^{2+}	5 / 0.1	2.0	2×10^{9}
R16	He^{2+}	5 / 0.1	2.0	5×10^{9}

Table II. Electronic properties for Z_1 and Z_2 estimated from Laplace-measurements, namely the energy position E, the effective electron capture cross section σ_n, the defect concentration N_t, and the effective minority carrier lifetime τ.

Trap label	E (eV)	σ_n (cm^{-2})	N_t (cm^{-3})
Z_1	E_c-0.58	4×10^{-15}	3×10^{-11}
Z_2	E_c- 0.65	6×10^{-15}	2×10^{-12}